

A&A manuscript no.

(will be inserted by hand later)

Your thesaurus codes are:

07(02.14.1; 08.01.1; 08.11.1; 10.01.1; 10.05.1; 10.19.1)

ASTRONOMY
AND
ASTROPHYSICS

Chemical composition of 90 F and G disk dwarfs [★]

Y.Q. Chen¹²³, P.E. Nissen¹, G. Zhao³, H.W. Zhang³⁴, and T. Benoni¹

¹ Institute of Physics and Astronomy, University of Aarhus, DK-8000 Aarhus C, Denmark

² Department of Astronomy, Beijing Normal University, Beijing 100875, P.R. China

³ Beijing Astronomical Observatory, Chinese Academy of Sciences, Beijing 100012, P.R. China

⁴ Department of Geophysics, Peking University, Beijing 100871, P.R. China

Received October 7 1999 / Accepted November 22 1999

Abstract. High resolution, high S/N spectra have been obtained for a sample of 90 F and G main-sequence disk stars covering the metallicity range $-1.0 < [\text{Fe}/\text{H}] < +0.1$, and have been analysed in a parallel way to the work of Edvardsson et al. (1993a) in order to re-inspect their results and to reveal new information on the chemical evolution of the Galactic disk.

Compared to Edvardsson et al. the present study includes several improvements. Effective temperatures are based on the Alonso et al. (1996) calibration of color indices by the infrared flux method and surface gravities are calculated from Hipparcos parallaxes, which also allow more accurate ages to be calculated from a comparison of M_V and T_{eff} with isochrones. In addition, more reliable kinematical parameters are derived from Hipparcos distances and proper motions in combination with accurate radial velocities. Finally, a larger spectral coverage, 5600 - 8800 Å, makes it possible to improve the abundance accuracy by studying more lines and to discuss several elements not included in the work of Edvardsson et al.

The present paper provides the data and discusses some general results of the abundance survey. A group of stars in the metallicity range of $-1.0 < [\text{Fe}/\text{H}] < -0.6$ having a small mean Galactocentric distance in the stellar orbits, $R_m < 7$ kpc, are shown to be older than the other disk stars and probably belong to the thick disk. Excluding these stars, a slight decreasing trend of $[\text{Fe}/\text{H}]$ with increasing R_m and age is found, but a large scatter in $[\text{Fe}/\text{H}]$ (up to 0.5 dex) is present at a given age and R_m . Abundance ratios with respect to Fe show, on the other hand, no significant scatter at a given $[\text{Fe}/\text{H}]$. The derived trends of O, Mg, Si, Ca, Ti, Ni and Ba as a function of $[\text{Fe}/\text{H}]$ agree rather well with those of Edvardsson et al., but the overabundance of Na and Al for metal-poor stars found in their work is not confirmed. Furthermore, the

Galactic evolution of elements not included in Edvardsson et al., K, V and Cr, is studied. It is concluded that the terms “ α elements” and “iron-peak elements” cannot be used to indicate production and evolution by specific nucleosynthesis processes; each element seems to have a unique enrichment history.

Key words: Nuclear reactions, nucleosynthesis, abundances – Stars: abundances – Stars: kinematics – Galaxy: abundances – Galaxy: evolution – Galaxy: solar neighbourhood

1. Introduction

The chemical abundances of long-lived F and G main sequence stars, combined with kinematical data and ages, provide a powerful way to probe the chemical and dynamical evolution of the Galaxy.

As far as the disk stars are concerned, many general trends have been discovered during the past decades. Most notable results are correlations of metallicity with age, Galactocentric distance, and vertical distance from the Galactic plane based on photometric or low-resolution observations (e.g. Eggen et al. 1962; Twarog 1980). In addition, the abundance patterns for some elements have been derived for small samples of stars: oxygen and α elements relative to iron vary systematically from overabundances at $[\text{Fe}/\text{H}] \simeq -1.0$ to a solar ratio at $[\text{Fe}/\text{H}] \simeq 0.0$, while most iron-peak elements follow iron for the whole metallicity range of the disk. These results have provided important constraints on chemical evolution models for the Galactic disk.

With improved observation and analysis techniques, which make it possible to study the Galactic chemical evolution (GCE) in detail, some old conclusions have, however, been challenged and new questions have arisen. Particularly important is the detailed abundance analysis of 189 F and G dwarfs with $-1.1 < [\text{Fe}/\text{H}] < 0.25$ by Edvardsson et al. (1993a, hereafter EAGLNT). The main results from this work may be summarized as follows: (1) There are no tight relations between age, metallicity and

Send offprint requests to: P.E. Nissen (pen@obs.aau.dk)

[★] Based on observations carried out at the Beijing Astronomical Observatory (Xinglong, P.R. China). Tables 3, 4 and 5 are only available in electronic form at the CDS via anonymous ftp to cdsarc.u-strasbg.fr (130.79.128.5) or via <http://cdsweb.u-strasbg.fr/Abstract.html>

kinematics of disk stars, but substantial dispersions imposed on weak statistical trends. (2) There exists a real scatter in the run of $[\alpha/\text{Fe}]$ vs. $[\text{Fe}/\text{H}]$ possibly due to the mixture of stars with different origins. The scatter seems to increase with decreasing metallicity starting at $[\text{Fe}/\text{H}] \simeq -0.4$. Together with a possible increase in the dispersion of W_{LSR} (the stellar velocity perpendicular to the Galactic plane with respect to the Local Standard of Rest, LSR) at this point, the result suggests a dual model for disk formation. It is, however, unclear if the transition at $[\text{Fe}/\text{H}] \simeq -0.4$ represents the division between the thin disk and the thick disk. (3) A group of metal-poor disk stars with $R_{\text{m}} < 7$ kpc is found to have larger $[\alpha/\text{Fe}]$ values than stars with $R_{\text{m}} > 9$ Kpc, indicating a higher star formation rate (SFR) in the inner disk than that in the outer disk. Since essentially all the oldest stars in EAGLNT have small R_{m} , it is, however, difficult to know upon which, R_{m} or age, the main dependence of $[\alpha/\text{Fe}]$ is. (4) At a given age and R_{m} , the scatter in $[\alpha/\text{Fe}]$ is negligible while $[\text{Fe}/\text{H}]$ does show a significant scatter. The former implies that the products of supernovae of different types are thoroughly mixed into the interstellar medium (ISM) before significant star formation occurs. Based on this, the large scatter in $[\text{Fe}/\text{H}]$ may be explained by infall of unprocessed gas with a characteristic mixing time much longer than that of the gas from supernovae of different types. (5) The Galactic scatter may be different for individual α elements; $[\text{Mg}/\text{Fe}]$ and $[\text{Ti}/\text{Fe}]$ show a larger scatter at a given metallicity than $[\text{Si}/\text{Fe}]$ and $[\text{Ca}/\text{Fe}]$. It suggests that individual α elements may have different origins. (6) A new stellar group, rich in Na, Mg, Al, was found among the metal-rich disk stars, suggesting additional synthesis sources for these elements.

Given that the study of EAGLNT was based on a limited sample of stars with certain selection effects and that the analysis technique induced uncertainties in the final abundances, some subtle results need further investigation before they can provide reliable constraints on theory. For example, it is somewhat unclear if the different $[\alpha/\text{Fe}]$ at a given metallicity between the inner disk and the outer disk stars is real and if old disk stars are always located in the inner disk. Moreover, recent work by Tomkin et al. (1997) argued against the existence of NaMgAl stars. In addition, a number of elements, which are highly interesting from a nucleosynthetic point of view, were not included in the work of EAGLNT.

The present work, based on a large differently selected sample of disk stars, aims at exploring and extending the results of EAGLNT with improved analysis techniques. Firstly, we now have more reliable atmospheric parameters. The effective temperature is derived from the Strömgren $b-y$ color index using a recent infrared-flux calibration and the surface gravity is based on the Hipparcos parallax. About one hundred iron lines (instead of ~ 30 in EAGLNT) are used to provide better determinations of metallicity and microturbulence. Secondly, the abundance

calculation is anchored at the most reliable theoretical or experimental oscillator strengths presently available in the literature. Thirdly, greater numbers of Fe II, Si I and Ca I lines in our study should allow better abundance determinations, and new elements (K, Sc, V, Cr and Mn) will give additional information on Galactic evolution. Lastly, the stellar age determination is based on new evolutionary tracks, and the space velocity is derived from more reliable distance and proper motion values.

In the following sections 2 to 6, we describe the observations and methods of analysis in details and present the derived abundances, ages and kinematics. The results are discussed in Sect. 7 and compared to those of EAGLNT. Two elements, Sc and Mn, not included in EAGLNT and represented by lines showing significant hyperfine structure (HFS) effects, are discussed in a separate paper (Nissen et al. 1999), which includes results for halo stars from Nissen & Schuster (1997).

2. Observations

2.1. Selection of stars

The stars were selected from the *uvby* - β photometric catalogues of Olsen (1983, 1993) according to the criteria of $5800 \leq T_{\text{eff}} \leq 6400$ K, $4.0 \leq \log g \leq 4.5$ and $-1.0 \leq [\text{Fe}/\text{H}] \leq +0.3$ with approximately equal numbers of stars in every metallicity interval of 0.1 dex. In this selection, the temperature was determined from the $b-y$ index with the calibration of Magain (1987), gravity was calculated from the c_1 index as described in EAGLNT, and metallicity was derived from the m_1 index using the calibrations of Schuster & Nissen (1989). The later re-determinations of the temperature with the calibration of Alonso et al. (1996) and the gravity from Hipparcos parallax lead to slight deviations from the selection criteria for some stars.

Based on the above selection, 104 F and G stars were observed, but 3 high-rotation ($V \sin i \geq 25 \text{ km s}^{-1}$) stars and 9 double-line spectroscopic binaries were excluded from the sample. Another 11 stars have radial velocity dispersions higher than the measurement error of the CORAVEL survey. HD 106516A and HD 97916 are suspected binaries (Carney et al. 1994), and HD 25998 and HD 206301 are possibly variables (e.g. Petit 1990; Morris & Mutel 1988). These 15 stars (marked in the column “Rem” of Table 3) are being carefully used in our study. The remaining stars are considered as single stars, but are checked for differences in iron abundances between Fe I and Fe II lines using gravities from Hipparcos parallaxes as suggested by Fuhrmann (1998). As described later, additional 2 stars were excluded during the analysis and thus the sample contains 90 stars for the final discussion and conclusions.

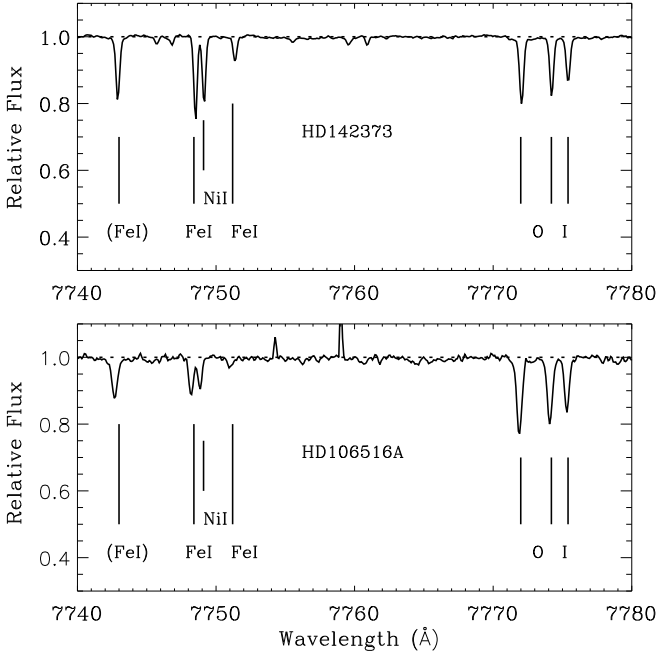


Fig. 1. Examples of spectra obtained with the 2.16m telescope at Xinglong Station for HD 142373 ($T_{\text{eff}} = 5920$ K, $\log g = 4.27$, $[\text{Fe}/\text{H}] = -0.39$) with a high S/N ~ 400 and HD 106516A ($T_{\text{eff}} = 6135$ K, $\log g = 4.34$, $[\text{Fe}/\text{H}] = -0.71$) with a relatively low S/N ~ 160 .

2.2. Observations and data reduction

The observations were carried out with the Coudé Echelle Spectrograph attached to the 2.16m telescope at Beijing Astronomical Observatory (Xinglong, P.R. China). The detector was a Tek CCD (1024×1024 pixels with $24 \times 24 \mu\text{m}^2$ each in size). The red arm of the spectrograph with a 31.6 grooves/mm grating was used in combination with a prism as cross-disperser, providing a good separation between the echelle orders. With a 0.5 mm slit (1.1 arcsec), the resolving power was of the order of 40 000 in the middle focus camera system.

The program stars were observed during three runs: March 21-27, 1997 (56 stars), October 21-23, 1997 (27 stars) and August 5-13, 1998 (21 stars). The exposure time was chosen in order to obtain a signal-to-noise ratio of at least 150 over the entire spectral range. Most bright stars have S/N $\sim 200 - 400$. Figure 1 shows the spectra in the region of the oxygen triplet for two representative stars HD 142373 and HD 106516A. In addition, the solar flux spectrum as reflected from the Moon was observed with a S/N ~ 250 and used as one of the “standard” stars in determining oscillator strengths for some lines (see Sect. 4.2).

The spectra were reduced with standard MIDAS routines for order identification, background subtraction, flat-field correction, order extraction and wavelength calibration. Bias, dark current and scattered light corrections

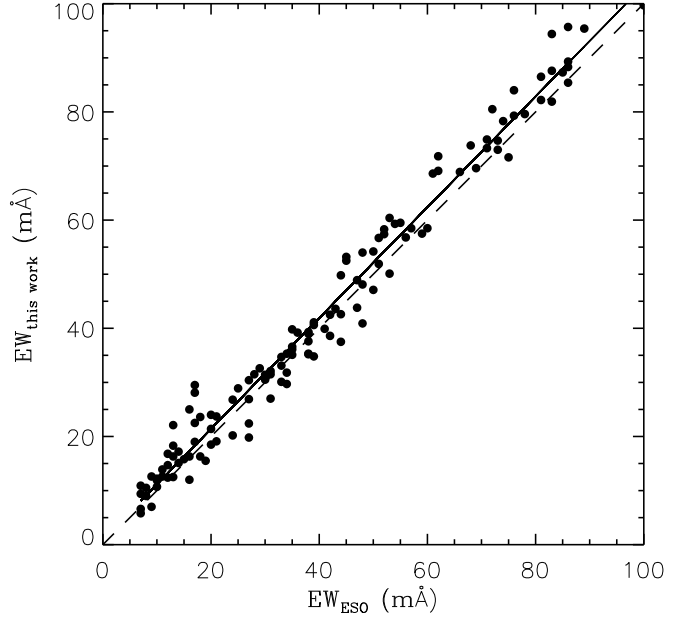


Fig. 2. A comparison of equivalent widths measured in this work with ESO data in EAGLNT for 5 stars in common. The thick line is the linear fit to the points, whereas the dashed line is the one-to-one relation.

are included in the background subtraction. If an early B-type star could be observed close to the program stars, it was used instead of the flat-field in order to remove interference fringes more efficiently. The spectrum was then normalized by a continuum function determined by fitting a spline curve to a set of pre-selected continuum windows estimated from the solar atlas. Finally, correction for radial velocity shift, measured from at least 20 lines, was applied before the measurement of equivalent widths.

2.3. Equivalent widths and comparison with EAGLNT

The equivalent widths were measured by three methods: direct integration, Gaussian and Voigt function fitting, depending on which method gave the best fit of the line profile. Usually, weak lines are well fitted by a Gaussian, whereas stronger lines in which the damping wings contribute significantly to their equivalent widths need the Voigt function to reproduce their profiles. If unblended lines are well separated from nearby lines, direct integration is the best method. In the case of some intermediate-strong lines, weighted averages of Gaussian and Voigt fitting were adopted.

The accuracy of the equivalent widths is estimated by comparing them to the independent measurements by EAGLNT for 25 stars in common. Five of them were observed at the ESO Observatory ($R \sim 60\,000$, S/N ~ 200) and 23 were observed at the McDonald Observatory ($R \sim 30\,000$, S/N $\sim 200 - 500$). The systematic difference

between the two sets of measurements is small and a linear least squares fitting gives:

$$\begin{aligned} EW_{X1} &= 1.025 (\pm 0.012) EW_{\text{ESO}} + 0.89 (\pm 0.56) \text{ (m\AA)} \\ EW_{X1} &= 1.083 (\pm 0.006) EW_{\text{McD}} - 0.94 (\pm 0.28) \text{ (m\AA)} \end{aligned}$$

The standard deviations around the two relations are 3.8 mÅ (for 129 lines in common with ESO) and 4.3 mÅ (for 575 lines in common with McDonald). Given that the error of the equivalent widths in EAGLNT is around 2 mÅ, we estimate an rms error of about 3 mÅ in our equivalent widths. As shown by the comparison of our equivalent widths with ESO data in Fig. 2, the equivalent widths below 50 mÅ are consistent with the one-to-one relation. The deviations for the stronger lines may be due to the fact that all lines in EAGLNT were measured by Gaussian fitting, which leads to an underestimate of equivalent widths for intermediate-strong lines because of neglecting their wings. We conclude that the Xinglong data may be more reliable than the EAGLNT data for lines in the range of $50 < EW < 100$ mÅ.

3. Stellar atmospheric parameters

3.1. Effective temperature and metallicity

The effective temperature was determined from the Strömgren indices ($b - y$ and c_1) and $[\text{Fe}/\text{H}]$ using the calibration of Alonso et al. (1996). If the color excess $E(b - y)$, as calculated from the H_β index calibration by Olsen (1988), is larger than 0.01, then a reddening correction was applied.

The metallicity, required in the input for temperature and abundance calculation, was first derived from the Strömgren m_1 index using the calibrations of Schuster & Nissen (1989). But the spectroscopic metallicity obtained later was used to iterate the whole procedure.

The errors of the photometric data are $\sigma(b - y) = 0.004$ and $\sigma(c_1) = 0.008$ according to Olsen (1993). Adopting $\sigma([\text{Fe}/\text{H}]) = 0.1$ from the spectroscopic analysis, the statistical error of T_{eff} is estimated to about ± 50 K. Considering a possible error of ± 50 K in the calibration, the error in temperature could reach ± 70 K. We do not adopt the excitation temperature, determined from a consistent abundance derived from Fe I lines with different excitation potentials, because errors induced by incorrect damping parameters (Ryan 1998) or non-LTE effects can be strongly dependent on excitation potential, leading to an error in effective temperature as high as 100 K.

3.2. Gravity

In most works, gravities are determined from the abundance analysis by requiring that Fe I and Fe II lines give the same iron abundance. But it is well known that the derivation of iron abundance from Fe I and Fe II lines may

be affected by many factors such as unreliable oscillator strengths, possible non-LTE effects and uncertainties in the temperature structure of the model atmospheres. From the Hipparcos parallaxes, we can determine more reliable gravities using the relations:

$$\log \frac{g}{g_\odot} = \log \frac{\mathcal{M}}{\mathcal{M}_\odot} + 4 \log \frac{T_{\text{eff}}}{T_{\text{eff},\odot}} + 0.4 (M_{\text{bol}} - M_{\text{bol},\odot}) \quad (1)$$

and

$$M_{\text{bol}} = V + BC + 5 \log \pi + 5, \quad (2)$$

where, \mathcal{M} is the stellar mass, M_{bol} the absolute bolometric magnitude, V the visual magnitude, BC the bolometric correction, and π the parallax.

The parallax is taken from the Hipparcos Satellite observations (ESA 1997). For most program stars, the relative error in the parallax is of the order of 5%. Only two stars in our sample have errors larger than 10%. From these accurate parallaxes, stellar distances and absolute magnitudes were obtained. Note, however, that our sample includes some binaries, for which the absolute magnitude from the Hipparcos parallax could be significantly in error. An offset of -0.75 mag will be introduced for a binary with equal components through the visual magnitude in Eq. (2). Thus, we also calculated absolute magnitudes from the photometric indices β and c_1 using the relations found by EAGLNT. Although the absolute magnitude of a binary derived by the photometric method is also not very accurate due to different spectral types and thus different flux distributions of the components, it may be better than the value from the parallax method. Hence, for a few stars with large differences in absolute magnitudes between the photometry and parallax determination, we adopt the photometric values.

The bolometric correction was interpolated from the new BC grids of Alonso et al. (1995) determined from line-blanketed flux distributions of ATLAS9 models. It is noted that the zero-point of the bolometric correction adopted by Alonso et al., $BC_\odot = -0.12$, is not consistent with the bolometric magnitude of the Sun, $M_{\text{bol},\odot} = 4.75$, recently recommended by the IAU (1999). But the gravity determination from the Eq. (1) only depends on the M_{bol} difference between the stars and the Sun and thus the zero-point is irrelevant.

The derivation of mass is described in Sect. 6. The estimated error of $0.05 M_\odot$ in mass corresponds to an error of 0.03 dex in gravity, while errors of 0.05 mag in BC and 70 K in temperature each leads to an uncertainty of 0.02 dex in $\log g$. The largest uncertainty of the gravity comes from the parallax. A typical relative error of 5% corresponds to an error of 0.04 dex in $\log g$. In total, the error of $\log g$ is less than 0.10 dex.

The surface gravity was also estimated from the Balmer discontinuity index c_1 as described in EAGLNT. We find a small systematical shift (about 0.1 dex) between the two sets of $\log g$, with lower gravities from

the parallaxes. There is no corresponding shift between $M_V(\text{par})$ and $M_V(\text{phot})$. The mean deviation is 0.03 mag only, which indicates that the systematic deviation in $\log g$ comes from the gravity calibration in EAGLNT.

3.3. Microturbulence

The microturbulence, ξ_t , was determined from the abundance analysis by requiring a zero slope of $[\text{Fe}/\text{H}]$ vs. EW . The large number of Fe I lines in this study enables us to choose a set of lines with accurate oscillator strengths, similar excitation potentials ($\chi_{\text{low}} \geq 4.0$ eV) and a large range of equivalent widths (10 – 100 mÅ) for the determination. With this selection, we hope to reduce the errors from oscillator strengths and potential non-LTE effects for Fe I lines with low excitation potentials. The error of the microturbulence is about 0.3 km s^{-1} .

The relation of ξ_t as a function of T_{eff} and $\log g$ derived by EAGLNT corresponds to about 0.3 km s^{-1} lower values than those derived from our spectroscopic analysis. No obvious dependence of the difference on temperature, gravity and metallicity can be found. In particular, the value for the Sun in our work is 1.44 km s^{-1} , also 0.3 km s^{-1} higher than the value of 1.15 found from the EAGLNT relation. The difference in ξ_t between EAGLNT and the present work is probably related to the difference in equivalent widths of intermediate-strong lines discussed in Sect. 2.3. EAGLNT measured these lines by fitting a Gaussian function and hence underestimated their equivalent widths, leading to a lower microturbulence.

Finally, given that the atmospheric parameters were not determined independently, the whole procedure of deriving T_{eff} , $\log g$, $[\text{Fe}/\text{H}]$ and ξ_t was iterated to consistency. The atmospheric parameters of 90 stars are presented in Table 3. The uncertainties of the parameters are: $\sigma(T_{\text{eff}}) = 70 \text{ K}$, $\sigma(\log g) = 0.1$, $\sigma([\text{Fe}/\text{H}]) = 0.1$, and $\sigma(\xi_t) = 0.3 \text{ km s}^{-1}$.

4. Atomic line data

4.1. Spectral lines

All unblended lines with symmetric profiles having equivalent widths larger than 20 mÅ in the solar atlas (Moore et al. 1966) were cautiously selected. The equivalent width limit ensures that lines are not disappearing in the most metal-poor disk stars at $[\text{Fe}/\text{H}] = -1.0$. Given that very weak lines would lead to an increase of random errors in the abundance determination and that too strong lines are very sensitive to damping constants, only weak and intermediate-strong lines with $3 < EW < 100 \text{ mÅ}$ in the stellar spectra were adopted in our abundance analysis except for potassium, for which only one line (K I $\lambda 7699$) with an equivalent width range of 50 – 190 mÅ, is available.

4.2. Oscillator strengths

Due to the large number of measurable lines in the spectra, Fe I lines were used for microturbulence determination and temperature consistency check. Hence, careful selection of oscillator strengths for them is of particular importance. Of many experimental or theoretical calculations of oscillator strengths for Fe I lines, only three sources with precise gf values were chosen. They are: Blackwell et al. (1982b; 1982c), O’Brien et al. (1991) and Bard & Kock (1991) or Bard et al. (1994). The agreements between these sources are very satisfactory, and thus mean $\log gf$ values were adopted if oscillator strengths are available in more than one of the three sources. A few oscillator strengths with large differences between these sources were excluded.

References for other elements are: O I (Lambert 1978), Na I (Lambert & Warner 1968), Mg I (Chang 1990), Al I (Lambert & Warner 1968), Si I (Garz 1973), K I (Lambert & Warner 1968), Ca I (Smith & Raggett 1981), Ti I (Blackwell et al. 1982a; 1986a), V I (Whaling et al. 1985), Cr I (Blackwell et al. 1986b), Fe II (Biémont et al. 1991; Hannaford et al. 1992), Ni I (Kostyk 1982; Wickliffe & Lawler 1997) and Ba II (Wiese & Martin 1980).

These experimental or theoretical gf values were inspected to see if they give reliable abundances by evaluating the deviation between the abundance derived from a given line and the mean abundance from all lines of the same species. A significant mean deviation in the same direction for all stars (excluding the suspected binaries) were used to correct the gf value. Lines with large deviations in different directions for different stars were discarded from the experimental or theoretical $\log gf$ list. The two sets of values are presented in columns “abs.” and “cor.” in Table 4. Based on these gf values, we derived abundances for 10 “standard” stars: HD 60319, HD 49732, HD 215257, HD 58551, HD 101676, HD 76349, HD 58855, HD 22484, the Sun and HD 34411A (in metallicity order). Oscillator strengths for lines with unknown gf values were then determined from an inverse abundance analysis of the above 10 stars, which are distributed in the metallicity range $-0.9 \leq [\text{Fe}/\text{H}] \leq 0.0$ dex and were observed at high S/N $\sim 250 - 400$. Generally, the gf values for a given line from different “standard” stars agree well, and a mean value (given in the column “dif” in Table 4) was thus adopted.

4.3. Empirical enhancement factor

It has been recognized for a long time that line broadening derived from Unsöld’s (1955) approximation to Van der Waals interaction is too weak, and an enhancement factor, E_γ , should be applied to the damping parameter, γ . Usually, enhancement factors of Fe I lines with excitation potential of the lower energy level (χ_{low}) less than 2.6 eV are taken from the empirical calibration by Simmons & Black-

well (1982). For Fe I lines with $\chi_{low} > 2.6$ eV, $E_\gamma = 1.4$ is generally used in abundance analysis. Recently, Anstee & O’Mara’s (1995) computed the broadening cross sections for s-p and p-s transitions and found that E_γ should be $2.5 \sim 3.2$ for lines with $\chi_{low} > 3.0$ eV, whereas lines with $\chi_{low} < 2.6$ eV have broadening cross sections more consistent with Simmons & Blackwell’s (1982) work.

Following EAGLNT and other works, we adopted Simmons & Blackwell’s (1982) E_γ for Fe I lines with $\chi_{low} < 2.6$ eV and $E_\gamma = 1.4$ for the remaining Fe I lines, while a value of 2.5 was applied for Fe II lines as suggested by Holweger et al. (1990). Enhancement factors for Na I, Si I, Ca I and Ba II were taken from EAGLNT (see references therein). Finally, a value of 1.5 was adopted for the K I, Ti I and V I lines considering their low excitation potentials, and a factor of 2.5 was applied to the remaining elements following Mäcke et al. (1975). The effects of changing these values by 50% on the derived abundances are discussed in Sect. 5.2.

The atomic line data are given in Table 4.

5. Abundances and their uncertainties

5.1. Model atmospheres and abundance calculations

The abundance analysis is based on a grid of flux constant, homogeneous, LTE model atmospheres, kindly supplied by Bengt Edvardsson (Uppsala). The models were computed with the MARCS code using the updated continuous opacities by Asplund et al. (1997) including UV line blanketing by millions of absorption lines and many molecular lines.

The abundance was calculated with the program EQWIDTH (also made available from the stellar atmospheric group in Uppsala) by requiring that the calculated equivalent width from the model should match the observed value. The calculation includes natural broadening, thermal broadening, van der Waals damping, and the microturbulent Doppler broadening. The mean abundance was derived from all available lines by giving equal weight to each line. Finally, solar abundances, calculated from the Moon spectrum, were used to derive stellar abundances relative to solar values (Table 5). Such differential abundances are generally more reliably than absolute abundances because many systematic errors nearly cancel out.

5.2. Uncertainties of abundances

There are two kinds of uncertainties in the abundance determination: one acts on individual lines, and includes random errors of equivalent widths, oscillator strengths, and damping constants; another acts on the whole set of lines with the main uncertainties coming from the atmospheric parameters.

5.2.1. Errors from equivalent widths and atomic data

The comparison of equivalent widths in Sect. 2.3 indicates that the typical uncertainty of the equivalent width is about 3 mÅ, which leads to an error of about 0.06 dex in the elemental ratio X/H derived from a single line with an equivalent width around 50 mÅ. For an element represented by N lines, the error is decreased by a factor \sqrt{N} . In this way, the errors from equivalent widths were estimated for elements with only one or a few lines. Alternatively, the scatter of the deduced abundances from a large number of lines with reliable oscillator strengths gives another estimate of the uncertainty from equivalent widths. With over 100 Fe I lines for most stars, the scatter varies somewhat from star to star with a mean value of 0.07 dex, corresponding to an error of 0.007 dex in [Fe/H]. Other elements with significant numbers of lines, such as Ca, Ni and Si, have even smaller mean line-to-line scatters.

The uncertainties in atomic data are more difficult to evaluate. But any error in the differential abundance caused by errors in the gf values is nearly excluded due to the correction of some experimental or theoretical gf values and the adoption of mean gf values from 10 “standard” stars. Concerning the uncertainties in the damping constants, we have estimated their effects by increasing the adopted enhancement factors by 50%. The microturbulence was accordingly adjusted because of the coupling between the two parameters. The net effect on the differential abundances with respect to the Sun is rather small as seen from Table 1.

5.2.2. Consistency check of atmospheric parameters

As a check of the photometric temperature, the derived iron abundance from individual Fe I lines was studied as a function of the excitation potential. To reduce the influence of microturbulence, only lines with equivalent widths less than 70 mÅ were included. A linear least squares fit to the abundance derived from each line vs. low excitation potential determines the slope in the relation $[\text{Fe}/\text{H}] = a + b \cdot \chi_{low}$. The mean slope coefficient for all stars is $b = 0.004 \pm 0.013$. There is only a very small (if any) dependence of b on effective temperature, surface gravity or metallicity. A suspected binary, HD 15814, has a very deviating slope coefficient ($b = -0.056$) and is excluded from further analysis.

The agreement of iron abundances derived from Fe I and Fe II lines is satisfactory when gravities based on Hipparcos parallaxes are used (see Fig. 3). The deviation is less than 0.1 dex for most stars with a mean value of -0.009 ± 0.07 dex. From $[\text{Fe}/\text{H}] = 0.0$ to $[\text{Fe}/\text{H}] = -0.5$, the mean deviation ($[\text{Fe}/\text{H}]_{\text{II}} - [\text{Fe}/\text{H}]_{\text{I}}$) seems, however, to increase by about 0.1 dex in rough agreement with predictions from non-LTE computations (see Sect. 5.3).

The deviation in iron abundances based on Fe I and Fe II abundance provides a way to identify binaries and

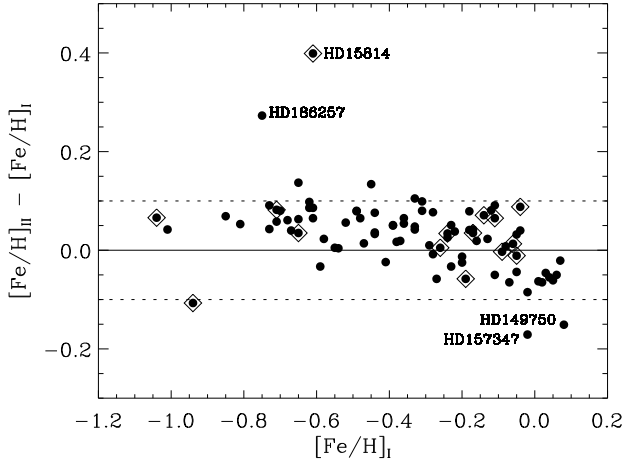


Fig. 3. Difference in iron abundances derived from Fe I and Fe II lines vs. $[\text{Fe}/\text{H}]$ with suspected binaries marked by a square around the filled circles.

to estimate the influence of the component on the primary. The suspected binaries are marked with an additional square around the filled circles in Fig. 3. It shows that there is no significant influence from the component for these binaries except in the case of HD 15814, which was already excluded on the basis of its b -coefficient in the excitation equilibrium of Fe I lines. Thus, the other possible binaries were included in our analysis. It is, however, surprising that HD 186257 show a higher iron abundance based on Fe II lines than that from Fe I lines with a deviation as large as 0.28 dex. We discard this star in the final analysis and thus have 90 stars left in our sample.

5.2.3. Errors in resulting abundances

Table 1 shows the effects on the derived abundances of a change by 70 K in effective temperature, 0.1 dex in gravity, 0.1 dex in metallicity, and 0.3 km s^{-1} in microturbulence, along with errors from equivalent widths and enhancement factors, for two representative stars.

It is seen that the relative abundances with respect to iron are quite insensitive to variations of the atmospheric parameters. One exception is $[\text{O}/\text{Fe}]$ due to the well known fact that the oxygen abundance derived from the infrared triplet has an opposite dependence on temperature to that of the iron abundance. After rescaling of our oxygen abundances to results from the forbidden line at $\lambda 6300$ (see next section) the error is somewhat reduced. Therefore, the error for $[\text{O}/\text{Fe}]$ in Table 1 might be overestimated.

In all, the uncertainties of the atmospheric parameters give errors of less than 0.06 dex in the resulting $[\text{Fe}/\text{H}]$ values and less than 0.04 dex in the relative abundance ratios. For an elemental abundance derived from many lines, this is the dominant error, while for an abundance derived from a few lines, the uncertainty in the equivalent

Table 1. Abundance errors. The last column gives the total error assuming that the individual errors are uncorrelated

HD142373 $T_{\text{eff}} = 5920$ $\log g = 4.27$ $[\text{Fe}/\text{H}] = -0.39$ $\xi_t = 1.48$							
	$\frac{\sigma_{EW}}{\sqrt{N}}$	ΔT_{eff}	$\Delta \log g$	$\Delta [\frac{\text{Fe}}{\text{H}}]$	$\Delta \xi_t$	ΔE_γ	σ_{tot}
		+70K	+0.1	+0.1	+0.3	50%	
$\Delta [\frac{\text{Fe}}{\text{H}}]$.009	.048	-.005	.001	-.040	.015	.065
$\Delta [\frac{\text{Fe}}{\text{H}}]_{II}$.030	-.012	.031	.018	-.046	.007	.067
$\Delta [\frac{\text{O}}{\text{Fe}}]$.035	-.104	.024	.004	.020	.013	.115
$\Delta [\frac{\text{Na}}{\text{Fe}}]$.042	-.017	.004	-.001	.034	.011	.058
$\Delta [\frac{\text{Mg}}{\text{Fe}}]$.042	-.018	-.005	.005	.019	.015	.052
$\Delta [\frac{\text{Al}}{\text{Fe}}]$.035	-.023	.003	-.001	.033	.015	.055
$\Delta [\frac{\text{Si}}{\text{Fe}}]$.015	-.026	.005	.003	.025	.015	.042
$\Delta [\frac{\text{Ca}}{\text{Fe}}]$.023	-.002	-.008	.002	-.005	.011	.028
$\Delta [\frac{\text{Ti}}{\text{Fe}}]$.024	.017	.004	.000	.023	.009	.039
$\Delta [\frac{\text{V}}{\text{Fe}}]$.035	.019	.004	.000	.031	.011	.051
$\Delta [\frac{\text{Cr}}{\text{Fe}}]$.035	-.007	.001	.000	.025	.015	.053
$\Delta [\frac{\text{Ni}}{\text{Fe}}]$.011	.002	.004	.003	.013	.023	.029
$\Delta [\frac{\text{Ba}}{\text{Fe}}]$.060	.039	-.008	.005	-.041	.012	.084
$\Delta [\frac{\text{K}}{\text{Fe}}]$.060	.013	-.024	.013	-.029	.012	.074
HD106516 $T_{\text{eff}} = 6135$ $\log g = 4.34$ $[\text{Fe}/\text{H}] = -0.71$ $\xi_t = 1.48$							
	$\frac{\sigma_{EW}}{\sqrt{N}}$	ΔT_{eff}	$\Delta \log g$	$\Delta [\frac{\text{Fe}}{\text{H}}]$	$\Delta \xi_t$	ΔE_γ	σ_{tot}
		+70 K	+0.1	+0.1	+0.3	50%	
$\Delta [\frac{\text{Fe}}{\text{H}}]_I$.012	.042	-.003	.006	-.029	.022	.057
$\Delta [\frac{\text{Fe}}{\text{H}}]_{II}$.023	.000	.032	.008	-.025	.016	.050
$\Delta [\frac{\text{O}}{\text{Fe}}]$.042	-.079	.017	-.003	.007	-.003	.091
$\Delta [\frac{\text{Na}}{\text{Fe}}]$.042	-.018	.002	-.003	.026	.013	.054
$\Delta [\frac{\text{Mg}}{\text{Fe}}]$.042	-.014	-.009	.001	.012	.022	.052
$\Delta [\frac{\text{Si}}{\text{Fe}}]$.019	-.021	.004	-.001	.019	.023	.041
$\Delta [\frac{\text{Ca}}{\text{Fe}}]$.015	-.001	-.009	.002	-.009	.014	.024
$\Delta [\frac{\text{Ti}}{\text{Fe}}]$.030	.010	.003	.000	.021	.010	.039
$\Delta [\frac{\text{V}}{\text{Fe}}]$.042	.014	.003	.000	.025	.006	.051
$\Delta [\frac{\text{Cr}}{\text{Fe}}]$.035	-.006	.001	-.001	.018	.034	.052
$\Delta [\frac{\text{Ni}}{\text{Fe}}]$.012	-.001	.002	-.001	.013	.029	.034
$\Delta [\frac{\text{Ba}}{\text{Fe}}]$.042	.041	-.012	.008	-.047	.008	.077
$\Delta [\frac{\text{K}}{\text{Fe}}]$.060	.016	-.026	.010	-.039	.024	.082

widths may be more significant. Note that the uncertainties of equivalent widths for V and Cr (possibly also Ti) might be underestimated given that their lines are generally weak in this work. In addition, with only one strong line for the K abundance determination, the errors from equivalent widths, microturbulence and atomic line data are relatively large.

Lastly, we have explored the HFS effect on one Al I line at $\lambda 6698$, one Mg I line at $\lambda 5711$, and two Ba II lines at $\lambda 6141$ and $\lambda 6496$. The HFS data are taken from three

sources: Biehl (1976) for Al, Steffen (1985) for Mg and François (1996) for Ba. The results indicate that the HFS effects are very small for all these lines with a value less than 0.01 dex.

5.3. Non-LTE effects and inhomogeneous models

The assumption of LTE and the use of homogeneous model atmospheres may introduce systematic errors, especially on the slope of various abundance ratios $[X/Fe]$ vs. $[Fe/H]$. These problems were discussed at quite some length by EAGLNT. Here we add some remarks based on recent non-LTE studies and computations of 3D hydrodynamical model atmospheres.

Based on a number of studies, EAGLNT concluded that the maximum non-LTE correction of $[Fe/H]$, as derived from Fe I lines, is 0.05 to 0.1 dex for metal-poor F and G disk dwarfs. Recently, Thévenin & Idiart (1999) computed non-LTE corrections on the order of 0.1 to 0.2 dex at $[Fe/H] = -1.0$. Fig. 3 suggests that the maximum correction to $[Fe/H]$ derived from Fe I lines is around 0.1 dex, but we emphasize that this empirical check may depend on the adopted T_{eff} calibration as a function of $[Fe/H]$.

The oxygen infrared triplet lines are suspected to be affected by non-LTE formation, because they give systematically higher abundances than forbidden lines. Recent work by Reetz (1999) indicates that non-LTE effects are insignificant (< 0.05 dex) for metal-poor and cool stars, but become important for warm and metal-rich stars. For stars with $[Fe/H] > -0.5$ and $T_{\text{eff}} > 6000$ K in our sample, non-LTE effects could reduce the oxygen abundances by 0.1-0.2 dex. For this reason, we use Eq. (11) of EAGLNT to scale the oxygen abundances derived from the infrared triplet to those derived by Nissen & Edvardsson (1992) from the forbidden $[O I] \lambda 6300$.

The two weak Na I lines ($\lambda 6154$ and $\lambda 6160$) used for our Na abundance determinations, are only marginally affected by deviations from LTE formation (Baumüller et al. 1998). The situation for Al may, however, be different. The non-LTE analysis by Baumüller & Gehren (1997) of one of the Al I lines used in the present work ($\lambda 6698$) leads to about 0.15 dex higher Al abundances for the metal-poor disk dwarfs than those calculated from LTE. No non-LTE study for the other two lines used in the present work is available. We find, however, that the derived Al abundances depend on T_{eff} with lower $[Al/Fe]$ for higher temperature stars. This may be due to the neglect of non-LTE effects in our work. Hence, we suspect that the trend of $[Al/Fe]$ vs. $[Fe/H]$ could be seriously affected by non-LTE effects.

The recent non-LTE analysis of neutral magnesium in the solar atmosphere by Zhao et al. (1998) and in metal-poor stars by Zhao & Gehren (1999) leads to non-LTE corrections of 0.05 dex for the Sun and 0.10 dex for a $[Fe/H] = -1.0$ dwarf, when the abundance of Mg is de-

rived from the $\lambda 5711$ Mg I line. Similar corrections are obtained for some of the other lines used in the present work. Hence, we conclude that the derived trend of $[Mg/Fe]$ vs. $[Fe/H]$ is not significantly affected by non-LTE.

The line-profile analysis of the K I resonance line at $\lambda 7699$ by Takeda et al. (1996) shows that the non-LTE correction is -0.4 dex for the Sun and -0.7 dex for Procyon. There are no computations for metal-poor stars, but given the very large corrections for the Sun and Procyon one may expect that the slope of $[K/Fe]$ vs. $[Fe/H]$ could be seriously affected by differential non-LTE effects between the Sun and metal-poor stars.

The non-LTE study of Ba lines by Mashonkina et al. (1999), which includes two of our three Ba II lines ($\lambda 5853$ and $\lambda 6496$), give rather small corrections (< 0.10 dex) to the LTE abundances, and the corrections are very similar for solar metallicity and $[Fe/H] \simeq -1.0$ dwarfs. Hence, $[Ba/Fe]$ is not affected significantly.

In addition to possible non-LTE effects, the derived abundances may also be affected by the representation of the stellar atmospheres by plane-parallel, homogeneous models. The recent 3D hydrodynamical model atmospheres of metal-poor stars by Asplund et al. (1999) have substantial lower temperatures in the upper photosphere than 1D models due to the dominance of adiabatic cooling over radiative heating. Consequently, the iron abundance derived from Fe I lines in a star like HD 84937 ($T_{\text{eff}} \simeq 6300$ K, $\log g \simeq 4.0$ and $[Fe/H] \simeq -2.3$) is 0.4 dex lower than the value based on a 1D model. Although the effect will be smaller in a $[Fe/H] \simeq -1.0$ star, and the derived abundance ratios are not so sensitive to the temperature structure of the model, we clearly have to worry about this problem.

5.4. Abundance comparison of this work with EAGLNT

A comparison in abundances between this work and EAGLNT for the 25 stars in common provides an independent estimate of the errors of the derived abundances. The results are summarized in Table 2.

The agreement in iron abundance derived from Fe I lines is satisfactory with deviations within ± 0.1 dex for the 25 common stars. These small deviations are mainly explained by different temperatures given the fact that the abundance differences increase with temperature deviations between the two works. The rms deviation in iron abundance derived from Fe II lines are slightly larger than that from Fe I lines. The usage of different gravities partly explain this. But the small line-to-line scatter from 8 Fe II lines in our work indicates a more reliable abundance than that of EAGLNT who used 2 Fe II lines only.

Our oxygen abundances are systematically higher by 0.15 dex than those of EAGLNT for 5 common stars. Clearly, the temperature deviation is the main reason. The systematically lower value of 70 K in our work increases $[O/Fe]$ by 0.10 dex (see Table 1).

Table 2. Mean abundance differences (this work–EAGLNT) and standard deviations. N is the number of stars, for which a comparison was possible

	$\langle \Delta \rangle$	σ	N
$[\text{Fe}/\text{H}]_I$	−0.020	0.068	25
$[\text{Fe}/\text{H}]_{II}$	−0.004	0.090	25
$[\text{O}/\text{Fe}]$	0.147	0.064	5
$[\text{Na}/\text{Fe}]$	−0.079	0.057	21
$[\text{Mg}/\text{Fe}]$	−0.020	0.080	21
$[\text{Al}/\text{Fe}]$	−0.033	0.080	16
$[\text{Si}/\text{Fe}]$	−0.012	0.054	23
$[\text{Ca}/\text{Fe}]$	0.055	0.039	25
$[\text{Ti}/\text{Fe}]$	−0.093	0.099	24
$[\text{Ni}/\text{Fe}]$	−0.008	0.045	25
$[\text{Ba}/\text{Fe}]$	0.068	0.081	25

The mean abundance differences for Mg, Al, Si, Ca and Ni between the two works are hardly significant. The systematical differences (this work – EAGLNT) of -0.08 dex for $[\text{Na}/\text{Fe}]$ and $[\text{Ti}/\text{Fe}]$ and $+0.07$ dex for $[\text{Ba}/\text{Fe}]$ are difficult to explain, but we note that when the abundances are based on a few lines only, a systematic offset of the stars relative to the Sun may occur simply because of errors in the solar equivalent widths.

6. Stellar masses, ages and kinematics

6.1. Masses and ages

As described in Sect. 3.2, the stellar mass is required in the determination of the gravity from the Hipparcos parallax. With the derived temperature and absolute magnitude, the mass was estimated from the stellar position in the $M_V - \log T_{\text{eff}}$ diagram (see Fig. 4) by interpolating in the evolutionary tracks of Vandenberg et al. (1999), which are distributed in metallicity with a step of ~ 0.1 dex. These new tracks are based on the recent OPAL opacities (Rogers & Iglesias 1992) using a varying helium abundance with $[\alpha/\text{Fe}] = 0.30$ for $[\text{Fe}/\text{H}] \leq -0.3$ and a constant helium abundance ($Y = 0.2715$) without α element enhancement for $[\text{Fe}/\text{H}] \geq -0.2$. Fig. 4 shows the position of our program stars with $-0.77 < [\text{Fe}/\text{H}] < -0.66$ compared to the evolutionary tracks of $Z = 0.004$ ($[\text{Fe}/\text{H}] = -0.71$). The errors in T_{eff} , M_V , and $[\text{Fe}/\text{H}]$ translate to an error of $0.06 M_{\odot}$ in the mass.

Stellar age is an important parameter when studying the chemical evolution of the Galaxy as a function of time. Specifically, the age is useful in order to interpret abundance ratios as a function of metallicity. In this work, the stellar age was obtained simultaneously with the mass from interpolation in the evolutionary tracks of Vandenberg et al. (1999). It was checked that practically the same age is derived from the corresponding isochrones. As an example, a set of stars are compared to isochrones in Fig. 5. The error of the age due to the uncertainties of

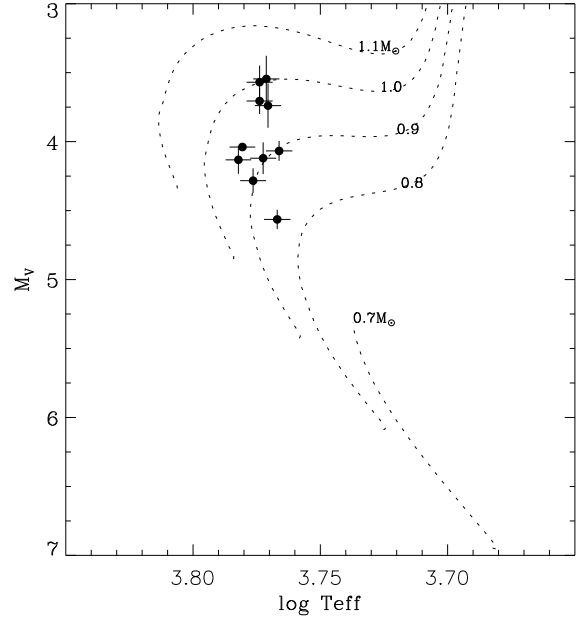


Fig. 4. The positions of our program stars with $-0.77 < [\text{Fe}/\text{H}] < -0.66$ compared to the evolutionary tracks of Vandenberg et al. (1999) with $[\text{Fe}/\text{H}] = -0.71$.

T_{eff} , M_V , and $[\text{Fe}/\text{H}]$ is about 15% ($\sigma(\log \tau) = 0.07$) except for a few stars, which have relatively large errors of the Hipparcos parallaxes.

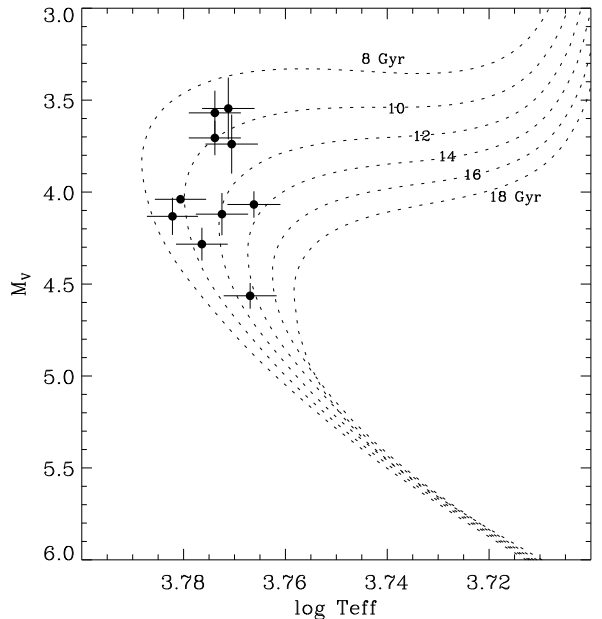


Fig. 5. The positions of our program stars with $-0.77 < [\text{Fe}/\text{H}] < -0.66$ compared to the isochrones of Vandenberg et al. (1999) with $[\text{Fe}/\text{H}] = -0.71$.

6.2. Kinematics

Stars presently near the Sun may come from a wide range of Galactic locations. Information on their origin will help us to understand their abundance ratios. Therefore, stellar space velocity, as a clue to the origin of a star in the Galaxy, is very interesting.

The accurate distance and proper motion available in the Hipparcos Catalogue (ESA 1997), combined with stellar radial velocity, make it possible to derive a reliable space velocity. Radial velocities from the CORAVEL survey for 53 stars were kindly made available by Nordström (Copenhagen) before publication. These velocities are compared with our values derived from the Doppler shift of spectral lines. A linear least squares fit for 40 stars (excluding the suspected binaries) gives:

$$RV = 0.997 (\pm 0.002) RV_{\text{CORAVEL}} + 0.26 (\pm 0.12) \text{ km s}^{-1}$$

The rms scatter around the relation is 0.72 km s^{-1} , showing that our radial velocities are as accurate as 0.5 km s^{-1} . Hence, our values are adopted for stars not included in the CORAVEL survey.

The calculation of the space velocity with respect to the Sun is based on the method presented by Johnson & Soderblom (1987). The correction of space velocity to the Local Standard of Rest is based on a solar motion, $(-10.0, +5.2, +7.2) \text{ km s}^{-1}$ in $(U, V, W)^1$, as derived from Hipparcos data by Dehnen & Binney (1998). The error in the space velocity arising from the uncertainties of distance, proper motion and radial velocity is very small with a value of about $\pm 1 \text{ km s}^{-1}$.

The ages and space velocities derived in the present work are generally consistent with EAGLNT. But the more accurate absolute magnitude, as well as the new set of theoretical isochrones, in our study should give more reliable ages than those determined by EAGLNT based on the photometric absolute magnitude and the old isochrones of Vandenberg & Bell (1985). This situation is also true for space velocities with our results based on distances and proper motions now available from Hipparcos.

7. Results and discussion

7.1. Relations between abundances, kinematics and ages

The observed trends between abundances, kinematics and ages are the most important information for theories of Galactic evolution. Especially, EAGLNT have provided many new results on this issue. For example, the substantial dispersion in the AMR found by EAGLNT argues against the assumption of chemical homogeneity adopted in many chemical evolution models. It is, however, important to test the results of EAGLNT for a different sample of disk stars. Based on more reliable ages and kinematics, the present study makes such an investigation.

¹ In the present work, U is defined to be positive in the anticentric direction.

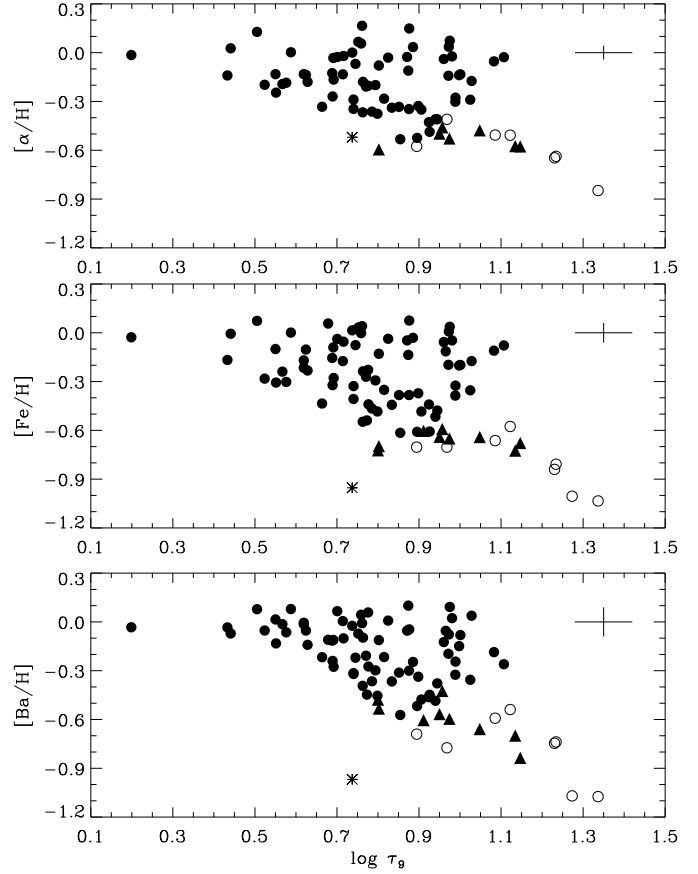


Fig. 6. The abundances of α elements, Fe and Ba as a function of logarithmic age. The symbols are shown in Fig. 7.

7.1.1. Age-metallicity relation in the disk

Fig. 6 shows the age-metallicity relations for α , iron² and barium elements, where α represents the mean abundance of Mg, Si, Ca and Ti. Generally, there is a loose correlation between age and abundance. Stars younger than 5 Gyr ($\log \tau_9 < 0.7$) are more metal-rich than $[\text{Fe}/\text{H}] \simeq -0.3$, and stars with $[\text{Fe}/\text{H}] < -0.5$ are not younger than 6–7 Gyr ($\log \tau_9 > 0.8$). The deviating young halo star HD 97916 (indicated by an asterisk in Fig. 6) is discussed in Sect. 8.

The correlation between age and abundance is, however, seriously distorted by a considerable scatter. Stars with solar metallicity have an age spread as large as 10 Gyr, and coeval stars at 10 Gyr show metallicity differences as high as 0.8 dex. Such a dispersion cannot be explained by either the abundance error (< 0.1 dex) or the age uncertainty ($\sim 15\%$) in the AMR. This is an im-

² Here and in the following sections and figures, the iron abundance is the mean abundance derived from all Fe I and Fe II lines with equal weight to each line.

portant constraint on GCE models, which must reproduce both the weak correlation and the substantial dispersion.

It is seen from Fig. 6 that Ba has the steepest slope in the AMR, Fe has intermediate slope, and the α elements show only a very weak trend with $[\text{Fe}/\text{H}]$. This was also found by EAGLNT and is consistent with nucleosynthesis theory that suggests that the main synthesis sites of Ba, Fe and α elements are AGB stars ($1\text{--}3 M_{\odot}$), SNe Ia ($6\text{--}8 M_{\odot}$) and SNe II ($> 8 M_{\odot}$), respectively. Due to their longer lifetime, lower mass stars contribute to the enrichment of the Galaxy at a later epoch, i.e. after massive stars have been polluting their products into the ISM. Hence, the Ba abundance is relatively low in the beginning of the disk evolution and increases quickly in the late stage, leading to a steeper slope.

It is interesting that there is a hint of a smaller metallicity spread for young stars with $\log \tau_9 = 0.4\text{--}0.8$ in this work than in EAGLNT, while the spread is similar for old stars. If we are not misled by our sample (less young stars than in the EAGLNT sample and a lack of stars with $\log \tau_9 < 0.4$), it seems that there are metal-rich stars at any time in the solar neighbourhood while metal-poor stars are always old. Another interesting feature for the young stars is that $[\text{Ba}/\text{H}]$ has a smaller metallicity spread than $[\text{Fe}/\text{H}]$ and $[\alpha/\text{H}]$. This could be due to the dependence of elemental yield on the progenitor's mass. Ba is produced by AGB stars with a rather small mass range of $1\text{--}3 M_{\odot}$, while Fe and α elements are synthesized by SNe having a mass range $\sim 6\text{--}30 M_{\odot}$.

7.1.2. Stellar kinematics as functions of age and metallicity

The study of the dispersion in kinematical parameters as a function of Galactic time is more interesting than the kinematical data alone, because any abrupt increase in dispersion may indicate special Galactic processes occurring during the evolution. Generally, dispersions in V_{LSR} , W_{LSR} and total velocity increase with stellar age. We have not enough stars at ~ 2.5 Gyr and 10 Gyr to confirm the abrupt increases in the W_{LSR} dispersion found by EAGLNT at these ages. Instead, our data seems to indicate that the kinematical dispersion (possibly also the metallicity) is fairly constant for stars younger than 5 Gyr ($\log \tau_9 = 0.7$), but it increases with age for stars with $\log \tau_9 > 0.7$. Coincidentally, 5 Gyr corresponds to $[\text{Fe}/\text{H}] \simeq -0.4$ dex, the metallicity where EAGLNT suggested an abundance transition related to a dual formation of the Galactic disk. The abundance transition at $[\text{Fe}/\text{H}] \simeq -0.4$ dex is confirmed by our data, but the increase of the W_{LSR} dispersion at $[\text{Fe}/\text{H}] \simeq -0.4$ found by EAGLNT is less obvious in our data.

When the velocity component in the direction of Galactic rotation, V_{LSR} , is investigated as a function of the metallicity (see Fig. 7), we find that there are two subpopulations for $[\text{Fe}/\text{H}] \leq -0.6$ with positive V_{LSR} in

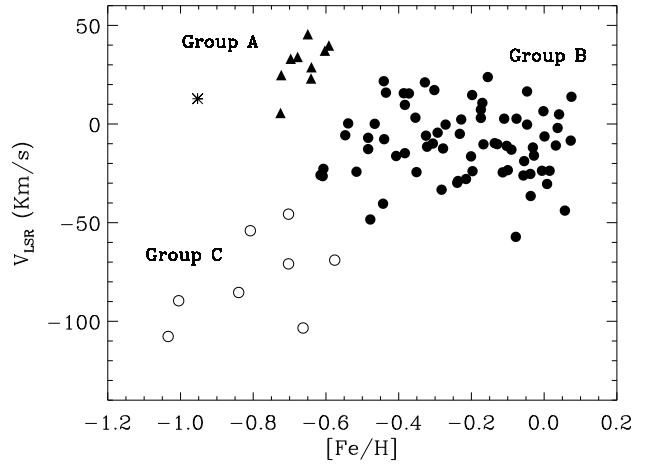


Fig. 7. V_{LSR} vs. $[\text{Fe}/\text{H}]$ with different symbols showing three groups of stars. The asterisk indicates the halo star HD 97916 discussed in Sect. 8.

group A and negative V_{LSR} in group C, while stars with $[\text{Fe}/\text{H}] \geq -0.6$ have V_{LSR} around $V_{\text{LSR}} = -10 \text{ km s}^{-1}$ (group B). The pattern persists when other elements are substituted for Fe. As shown in Edvardsson et al. (1993b), there is a tight correlation between V_{LSR} and the mean Galactocentric distance in the stellar orbit, R_m . Hence, we can trace the metallicity at different Galactocentric distances assuming that R_m is a reasonable estimator of the radius of the star's original orbit. Note, however, that the lower metallicity toward the Galactic center ($V_{\text{LSR}} \lesssim -50 \text{ km s}^{-1}$) for group C stars may be due to their large ages. Excluding these stars, a trend of decreasing metallicity with increasing V_{LSR} for stars with similar age is found, which indicates a radial abundance gradient in the disk, and thus suggests a faster evolution in the inner disk than the outer. This is compatible with a higher SFR, due to the higher density, in the inner disk.

There are two possibilities to explain the stars in group C. One is anchored to the fact that the oldest stars (> 10 Gyr) in our sample have the lowest V_{LSR} , i.e. the smallest R_m , indicating that the Galaxy did not extend to the Sun at 10 Gyr ago according to an inside-out formation process of the Galaxy. The other is that these stars come from the thick disk, which is older and more metal-poor than the thin disk.

7.2. Relative abundances

The general trends of elemental abundance with respect to iron as a function of metallicity, age and kinematics are to be studied in connection with Galactic evolution models and nucleosynthesis theory. The main results are shown in Fig. 8 and will be discussed together with those of EAGLNT.

7.2.1. Oxygen and magnesium

In agreement with most works, $[\text{O}/\text{Fe}]$ shows a tendency to decrease constantly with increasing metallicity for disk stars. As oxygen is only produced in the massive progenitors of SNe II, Ib and Ic, it is mainly build up at early times of the Galaxy, leading to an overabundance of oxygen in halo stars. The $[\text{O}/\text{Fe}]$ ratio gradually decline in the disk stars when iron is produced by the long-lived SNe Ia. The time delay of SNe Ia relative to SNe II is responsible for the continuous decrease of oxygen in disk stars. The tendency for $[\text{O}/\text{Fe}]$ to continue to decrease at $[\text{Fe}/\text{H}] > -0.3$ argues for an increasing ratio of SNe Ia to SNe II also at the later stages of the disk evolution.

In general, the relation of $[\text{O}/\text{Fe}]$ vs. V_{LSR} reflects the variation of $[\text{Fe}/\text{H}]$ with V_{LSR} (see Fig. 7). $[\text{O}/\text{Fe}]$ decreases with increasing V_{LSR} for stars with $V_{\text{LSR}} < 0$ and slowly increase with further larger V_{LSR} . Considering their similar ages, the decreasing $[\text{O}/\text{Fe}]$ from group A to group B stars may be attributed to the increasing V_{LSR} , whereas the higher $[\text{O}/\text{Fe}]$ of group C is due to an older age.

The magnesium abundance shows a decreasing trend with increasing metallicity like oxygen for $[\text{Fe}/\text{H}] < -0.3$ but it tends to flatten out for higher metallicities. Given that magnesium is theoretically predicted to be formed only in SNe II, the similar decreasing trend as oxygen is easily understood, but the flat $[\text{Mg}/\text{Fe}]$ towards higher metallicities than $[\text{Fe}/\text{H}] > -0.3$ is unexpected. It seems that SNe II are not the only source for Mg. Perhaps SNe Ia also contribute to the enrichment of Mg during disk evolution.

The flat trend of $[\text{Mg}/\text{Fe}]$ vs. $[\text{Fe}/\text{H}]$ for $[\text{Fe}/\text{H}] > -0.3$ is also evident from the data of EAGLNT if the high Mg/Fe ratios of their NaMgAl stars are reduced to a solar ratio as found by Tomkin et al. (1997). Feltzing and Gustafsson (1999) also find $[\text{Mg}/\text{Fe}]$ to be independent of metallicity for their more metal-rich stars although the scatter is large.

With more magnesium lines in the present study, we get a similar scatter of $[\text{Mg}/\text{Fe}]$ as EAGLNT. The scatter is slightly larger than that of oxygen and in particular much larger than those of Si and Ca. Although we do not find a large line-to-line scatter in the Mg abundance determination, it is still unclear if the scatter in $[\text{Mg}/\text{Fe}]$ is cosmic. Only 3 Mg I lines are available for most stars while Si and Ca are represented by 20-30 lines. There is no obvious evidence showing the scatter to be an effect of different V_{LSR} . Nor do we find a clear separation of thick disk stars from thin disk stars in the diagram of $[\text{Mg}/\text{Fe}]$ vs. $[\text{Mg}/\text{H}]$, as has been found by Fuhrmann (1998). It seems that neither observation nor theory is satisfactory for Mg.

7.2.2. Silicon, calcium and titanium

Like magnesium, $[\text{Si}/\text{Fe}]$ and $[\text{Ca}/\text{Fe}]$ decrease with increasing metallicity for $[\text{Fe}/\text{H}] < -0.4$ and then flatten out with further increasing $[\text{Fe}/\text{H}]$. The result is in agreement with EAGLNT, who found a “kink” at $[\text{Fe}/\text{H}] = -0.3 \sim -0.2$. But $[\text{Ca}/\text{Fe}]$ possibly continues to decrease for $[\text{Fe}/\text{H}] > -0.4$ based on our data. The suspicion that Si is about 0.05 dex overabundant relative to Ca for $[\text{Fe}/\text{H}] > -0.2$ and the possible upturn of silicon at higher metallicity in EAGLNT are not supported by our data.

Both Si and Ca have a very small star-to-star scatter (0.03 dex) at a given metallicity for thin disk stars. The scatter is slightly larger among the thick disk stars. Since the scatter corresponds to the expected error from the analysis, we conclude that the Galactic scatter for $[\text{Si}/\text{Fe}]$ and $[\text{Ca}/\text{Fe}]$ is less than 0.03 dex in the thin disk.

$[\text{Ti}/\text{Fe}]$ was shown by EAGLNT to be a slowly decreasing function of $[\text{Fe}/\text{H}]$ and the decrease continues to higher metallicity. Our data show a similar trend but the continuous decrease toward higher metallicity is less obvious with a comparatively large star-to-star scatter. There is no evidence that the scatter is correlated with V_{LSR} . We note that Feltzing & Gustafsson (1999) find a similar scatter in $[\text{Ti}/\text{Fe}]$ for metal-rich stars with the Ti abundance based on 10-12 Ti I lines.

7.2.3. Sodium and aluminum

Na and Al are generally thought to be products of Ne and C burning in massive stars. The synthesis is controlled by the neutron flux which in turn depends on the initial metallicity and primarily on the initial O abundance. Therefore, one expects a rapid increase of $[\text{Na}/\text{Mg}]$ and $[\text{Al}/\text{Mg}]$ with metallicity. But our data shows that both Na and Al are poorly correlated with Mg in agreement with EAGLNT. This means that the odd-even effect has been greatly reduced in the nucleosynthesis processes during the disk formation.

When iron is taken as the reference element, we find that $[\text{Na}/\text{Fe}]$ and $[\text{Al}/\text{Fe}]$ are close to zero for $[\text{Fe}/\text{H}] < -0.2$, while EAGLNT found 0.1-0.2 dex differences between $[\text{Fe}/\text{H}] = -0.2$ and $[\text{Fe}/\text{H}] = -1.0$. Our results support the old data by Wallerstein (1962) and Tomkin et al. (1985), who suggested $[\text{Na}/\text{Fe}] \sim 0.0$ for the whole metallicity range of the disk stars. The situation is the same for Al; EAGLNT found an overabundance of $[\text{Al}/\text{Fe}] \simeq 0.2$ for $[\text{Fe}/\text{H}] < -0.5$, whereas we find a solar ratio for the low metallicity stars. As discussed in Sect. 5.3 this may, however, be due to a non-LTE effect.

In the case of the more metal rich stars the abundance results for Na and Al are rather confusing. EAGLNT found that some metal-rich stars in the solar neighbourhood are rich in Na, Mg and Al, but the existence of such NaMgAl stars was rejected by Tomkin et al. (1997). Several further studies, however, confirmed the overabun-

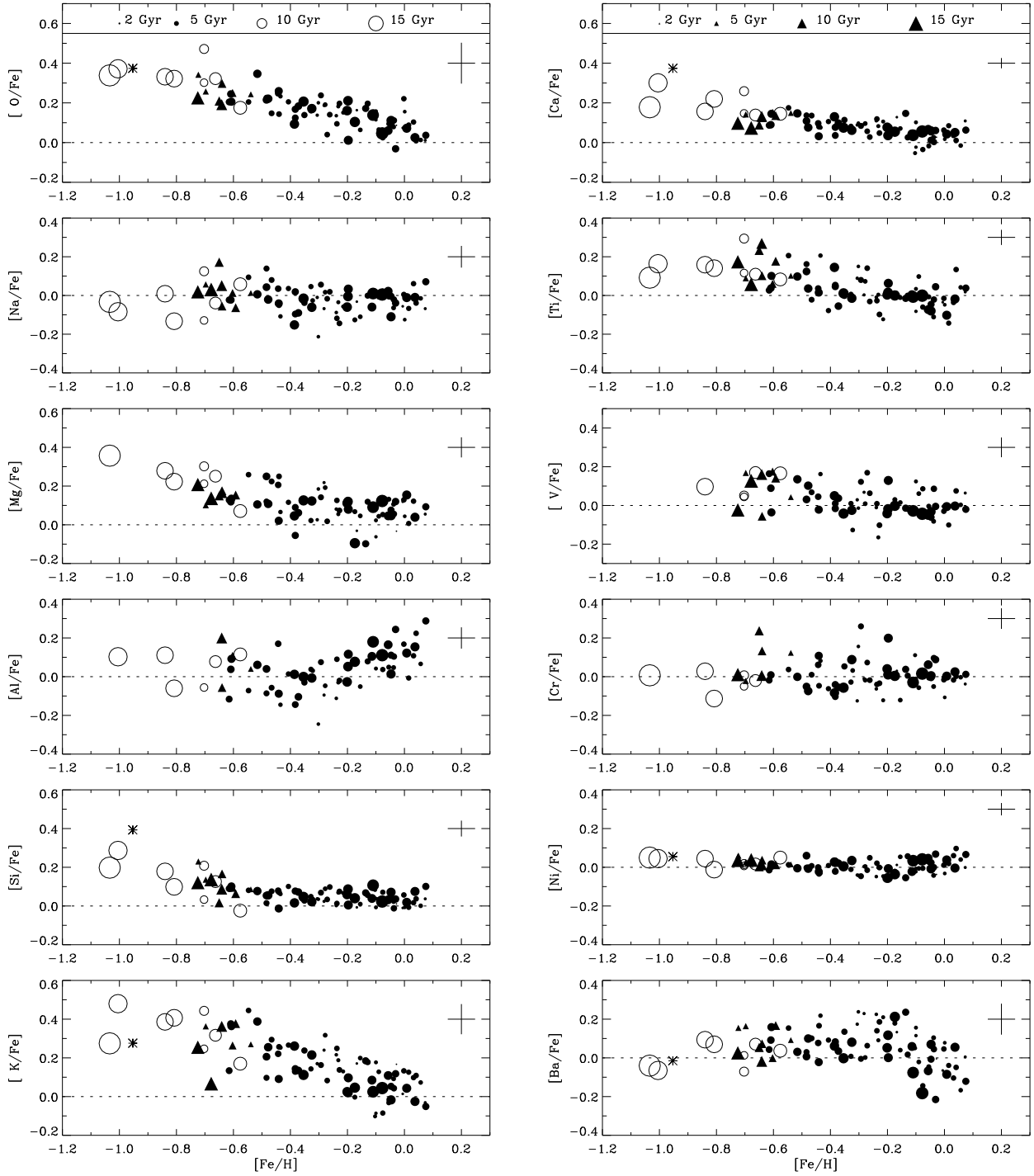


Fig. 8. Abundance patterns for elements from O to Ba. The symbols are the same as in Fig. 7 and their size is proportional to stellar age. Note that the trends of $[\text{Al}/\text{Fe}]$ and $[\text{K}/\text{Fe}]$ may be spurious due to the neglect of non-LTE effects.

dance of some elements again. Porte de Morte (1996) found an overabundance of Mg but not of Na. Feltzing & Gustafsson (1999) confirmed the upturn of $[\text{Na}/\text{Fe}]$ but their metal-rich stars did not show Mg and Al overabundances. In the present work we find a solar ratio of Na/Fe

up to $[\text{Fe}/\text{H}] \simeq 0.1$, and a rather steep upturn of $[\text{Al}/\text{Fe}]$ beginning at $[\text{Fe}/\text{H}] \simeq -0.2$. As discussed in Sect. 5.3, our Al abundances may, however, be severely affected by non-LTE effects. We conclude that more accurate data on Na and Al abundances are needed.

7.2.4. Potassium

$[K/Fe]$ shows a decreasing trend with increasing metallicity for disk stars. The result supports the previous work by Gratton & Sneden (1987) but our data have a smaller scatter. Assuming that potassium is a product of explosive oxygen burning in massive stars, Samland (1998) reproduces the observed trend rather well. Timmes et al. (1995), on the other hand, predicts $[K/Fe] < 0.0$ for $[Fe/H] < -0.6$ in sharp contrast to the observations. Given that the K I resonance line at $\lambda 7699$, which are used to derive the K abundances, is affected by non-LTE as discussed in Sect. 5.3, it seems premature to attribute K to one of α elements.

7.2.5. Vanadium, chromium and nickel

V and Cr seem to follow Fe for the whole metallicity range with some star-to-star scatter. The scatter is not a result of mixing stars with different V_{LSR} , and the few very weak lines used to determine the abundances prevent us to investigate the detailed dependence on metallicity and to decide if the scatter is cosmic or due to errors.

Ni follows iron quite well at all metallicities with a star-to-star scatter less than 0.03 dex. Two features may be found after careful inspection. Firstly, there is a hint that $[Ni/Fe]$ slightly decreases with increasing metallicity for $-1.0 < [Fe/H] < -0.2$. The trend is more clear, due to smaller star-to-star scatter, than in EAGLNT. Secondly, there is a subtle increase of $[Ni/Fe]$ for $[Fe/H] > -0.2$. Interestingly, Feltzing & Gustafsson (1999) found a slight increase of $[Ni/Fe]$ towards even more metal-rich stars.

7.2.6. Barium

The abundance pattern of Ba is very similar to that of EAGLNT except for a systematic shift of about +0.07 dex in $[Ba/Fe]$. Both works indicate a complicated dependence of $[Ba/Fe]$ on metallicity. First, $[Ba/Fe]$ seems to increase slightly with metallicity for $[Fe/H] < -0.7$, and then keeps a constant small overabundance until $[Fe/H] \sim -0.2$, after which $[Ba/Fe]$ decreases towards higher metallicities.

Barium is thought to be synthesized by neutron capture s-process in low mass AGB stars with an evolutionary timescale longer than that of iron-producing SNe Ia. Therefore, $[Ba/Fe]$ is still slightly underabundant at $[Fe/H] = -1.0$. Ba is then enriched significantly at later stages of the disk evolution, but the decrease of $[Ba/Fe]$ for more metal-rich stars beginning with $[Fe/H] \sim -0.2$ is unexpected.

Given that the low $[Ba/Fe]$ for some stars may be related to their ages, the relation of $[Ba/Fe]$ vs. $[Fe/H]$ at different age ranges was investigated (see Fig. 9). In agreement with EAGLNT, the run of $[Ba/Fe]$ vs. $[Fe/H]$ in old stars with $\log \tau_9 > 0.9$ (~ 8 Gyr) and $0.7 < \log \tau_9 < 0.9$ shows a flat distribution for $[Fe/H] < -0.3$ and a negative

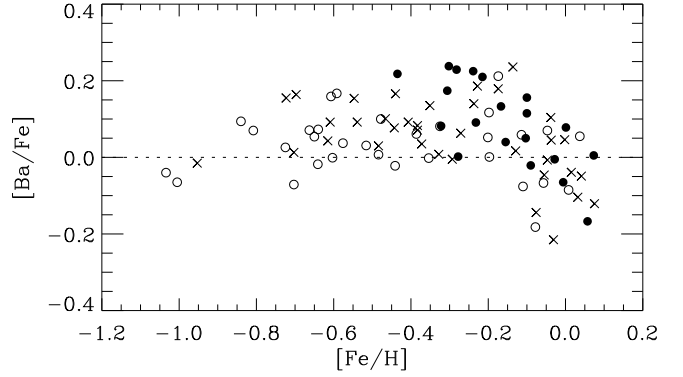


Fig. 9. Different relations of $[Ba/Fe]$ vs. $[Fe/H]$ for stars with different age ranges: $\log \tau_9 < 0.7$ (filled circles), $\log \tau_9 = 0.7 - 0.9$ (crosses) and $\log \tau_9 > 0.9$ (open circles).

slope for $[Fe/H] > -0.3$. All young stars with $\log \tau_9 < 0.7$ (~ 5 Gyr) have $[Fe/H] > -0.3$ and a clear decreasing trend of $[Ba/Fe]$ with $[Fe/H]$ is seen. In addition, there is a hint of higher $[Ba/Fe]$ for younger stars both in the interval $-0.7 < [Fe/H] < -0.3$, where $[Ba/Fe]$ is constant and in the interval $[Fe/H] > -0.3$, where $[Ba/Fe]$ is decreasing. This is consistent with the formation of young stars at a later stage of the disk when long-lived AGB stars have enhanced Ba in the ISM. The flat $[Ba/Fe]$ for $[Fe/H] < -0.3$ may be explained by the suggestion of EAGLNT that the synthesis of Ba in AGB stars is independent of metallicity, i.e. that Ba shows a primary behaviour during the evolution of the disk. But the age effect alone cannot explain the underabundant $[Ba/Fe]$ in metal-rich stars, because $[Ba/Fe]$ decreases with metallicity for all ages after $[Fe/H] = -0.3$. One reason could be that s-element synthesis occurs less frequently in metal-rich AGB stars possibly because the high mass loss finishes their evolution earlier.

8. Concluding remarks

One of the interesting results of this study is that the oldest stars presently located in the solar neighbourhood have $V_{LSR} \lesssim -50 \text{ km s}^{-1}$. Hence, they probably originate from the inner disk having $R_m < 7$ kpc. This is not coincidentally found in our study. The EAGLNT sample contains about 20 such stars. As shown in both works, these stars are generally more metal-poor than other stars and they show a larger spread in $[Fe/H]$ and $[Ba/H]$ than in $[\alpha/H]$ (see Fig. 6). According to EAGLNT, they have higher $[\alpha/Fe]$ than other disk stars at a metallicity about $[Fe/H] = -0.7$.

Considering these different properties, we suggest that they do not belong to the thin disk. Firstly, they are older (10-18 Gyr) than other stars. Secondly, if they are thin disk stars, it is hard to understand why stars coming from both sides of the solar annulus have lower metallicity than the local region. Thirdly, these stars show a

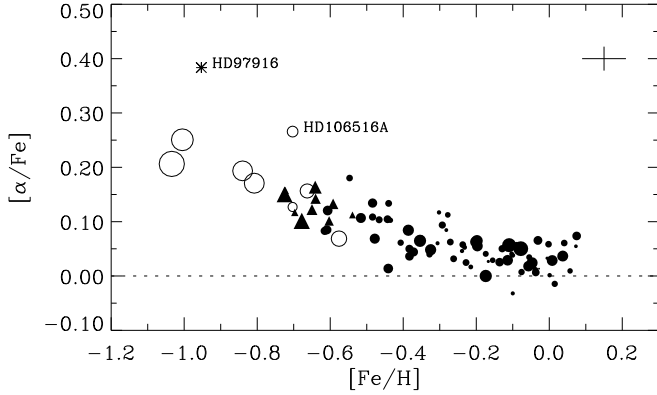


Fig. 10. The mean α (Mg, Si, Ca and Ti) abundance as a function of metallicity. The symbols are the same as in Fig. 7 and their size is proportional to stellar age.

relatively small metallicity dispersion at such early Galactic time, i.e. smaller than stars at 8-10 Gyr. This is not in agreement with the effect of orbital diffusion working during the evolution of the thin disk, which suggests larger metallicity dispersion for older stars. Finally, the W_{LSR} dispersion of these stars is about 40 km s^{-1} , considerably larger than the typical value of about 20 km s^{-1} for thin disk stars. Consistently, the kinematics, age, metallicity and abundance ratios of these stars follow the features of the thick disk: $V_{\text{LSR}} \lesssim -50 \text{ km s}^{-1}$, $\sigma(W_{\text{LSR}}) \simeq 40 \text{ km s}^{-1}$, $\tau > 10 \text{ Gyr}$, $[\text{Fe}/\text{H}] < -0.5$ and $[\alpha/\text{Fe}] \sim 0.2$. We conclude that these oldest stars in both EAGLNT and this work are thick disk stars. Hence, they are probably not resulting from an inside-out formation of the Galactic disk, but have been formed in connection with a merger of satellite components with the Galaxy.

Concerning the abundance connection of the thick disk with the thin disk, our data for $[\alpha/\text{Fe}]$, shown in Fig. 10, suggest a more smooth trend than those of EAGLNT, who found a correlation between $[\alpha/\text{Fe}]$ and R_{m} at $[\text{Fe}/\text{H}] \sim -0.7$. We leave the issue open considering the small number of these stars in our work. Two stars marked by their names in Fig. 10 may be particularly interesting because they show significantly higher $[\alpha/\text{Fe}]$ than other stars. Fuhrmann & Bernkopf (1999) suggest that one of them, HD 106516A, is a thick-disk field blue straggler. It is unclear if this can explain the higher $[\alpha/\text{Fe}]$. HD 97916 is a nitrogen rich binary (Beveridge & Sneden 1994) with $U_{\text{LSR}} = -117 \text{ km s}^{-1}$ and $W_{\text{LSR}} = 101 \text{ km s}^{-1}$ (typical for halo stars), but with $V_{\text{LSR}} = 22 \text{ km s}^{-1}$ similar to the value for thin disk stars. Surprisingly, this star is also very young (5.5 Gyr) for its metallicity.

It is interesting to re-inspect the observational results for thin disk stars excluding the thick disk stars. More direct information on the evolution of the Galactic thin disk will be then obtained. In summary, the thin disk is younger (not older than 12 Gyr), more metal-rich ($[\text{Fe}/\text{H}] > -0.8$) and has a smaller $[\alpha/\text{Fe}]$ spread (0.1 dex) without the

mixture of the thick disk stars. In particular, the AMR is more weak and there seems to exist a radial metallicity gradient. All these features agree better with the present evolutionary models for the Galactic disk.

We emphasize here that there is no obvious gradient in $[\alpha/\text{Fe}]$ for the thin disk at a given metallicity. Such a gradient was suggested by EAGLNT based on higher $[\alpha/\text{Fe}]$ of the oldest stars with $R_{\text{m}} < 7 \text{ kpc}$ than stars with $R_{\text{m}} > 7 \text{ kpc}$ (see their Fig. 21). After we have ascribed these oldest stars to the thick disk, the abundance gradient disappears.

Our study of relative abundance ratios as a function of $[\text{Fe}/\text{H}]$ suggests that there are subtle differences of origin and enrichment history both within the group of α elements and the iron-peak elements. Nucleosynthesis theory predicts that Si and Ca are partly synthesized in SNe Ia, while O and Mg are only produced in SNe II (Tsujimoto et al. 1995). Our data suggest, however, that SNe Ia may also be a significant synthesis site of Mg, because $[\text{Mg}/\text{Fe}]$ shows a trend more similar to $[\text{Si}/\text{Fe}]$ and $[\text{Ca}/\text{Fe}]$ than to $[\text{O}/\text{Fe}]$. Ti may not lie in a smooth extension of Si and Ca, because there is a hint of a decrease of $[\text{Ti}/\text{Fe}]$ for $[\text{Fe}/\text{H}] > -0.4$ not seen in the case of Si and Ca. The situation for the odd-Z elements is more complicated. The available data for Na and Al show confusing disagreements; EAGLNT finds an overabundance of 0.1 to 0.2 dex for $[\text{Na}/\text{Fe}]$ and $[\text{Al}/\text{Fe}]$ among the metal-poor disk stars, whereas our study points at solar ratios. Two other odd-Z elements, K and Sc (Nissen et al. 1999), behave like α elements, but the result for K is sensitive to the assumption of LTE. The iron-peak elements also show different behaviours: V, Cr and Ni follow Fe very well, while $[\text{Mn}/\text{Fe}]$ (Nissen et al. 1999) decreases with decreasing metallicity from $[\text{Mn}/\text{Fe}] \simeq 0.0$ at $[\text{Fe}/\text{H}] = 0.0$ to $[\text{Mn}/\text{Fe}] \simeq -0.4$ at $[\text{Fe}/\text{H}] = -1.0$. We conclude that the terms “ α elements” and “iron-peak elements” do not indicate productions in single processes, and that each element seems to have a unique enrichment history.

Acknowledgements

This research was supported by the Danish Research Academy and the Chinese Academy of Sciences. Bengt Edvardsson is thanked for providing a grid of the Uppsala new MARCS model atmospheres, and Birgitta Nordström for communicating CORAVEL radial velocities in advance of publication.

References

- Alonso A., Arribas S., Martínez-Roger C., 1995, *A&A* 297, 197
- Alonso A., Arribas S., Martínez-Roger C., 1996, *A&A* 313, 873
- Anstee S.D., O’Mara B.J., 1995, *MNRAS* 276, 859
- Asplund M., Gustafsson B., Kiselman D., Eriksson K., 1997, *A&A* 318, 521
- Asplund M., Nordlund Å., Trampedach R., Stein R.F., 1999, *A&A* 346, L17

- Bard A., Kock M., 1994, *A&A* 282, 1014
- Bard A., Kock A., Kock M., 1991, *A&A* 248, 315
- Baumüller D., Butler K., Gehren T., 1998, *A&A* 338, 637
- Baumüller D., Gehren T., 1997, *A&A* 325, 1088
- Beveridge C.R., Sneden C., 1994, *AJ* 108, 285
- Biémont E., Baudoux M., Kurucz R.L., Ansbacher W., Pinnington E.H., 1991, *A&A* 249, 539
- Biehl D., 1976, Diplomarbeit, Inst. f. Theor. Physik u. Sternwarte, Kiel University
- Blackwell D.E., Booth A.J., Menon S.L.R., Petford A.D., 1986a, *MNRAS* 220, 289
- Blackwell D.E., Booth A.J., Menon S.L.R., Petford A.D., 1986b, *MNRAS* 220, 303
- Blackwell D.E., Menon S.L.R., Petford A.D., Shallis M.J., 1982a, *MNRAS* 201, 611
- Blackwell D.E., Petford A.D., Shallis M.J., Simmons G.J., 1982b, *MNRAS* 199, 43
- Blackwell D.E., Petford A.D., Simmons G.J., 1982c, *MNRAS* 201, 595
- Carney B.W., Latham D.W., Laird J.B., Aguilar L.A., 1994, *AJ* 107, 2240
- Chang T.N., 1990, *Phys. Rev. A* 41, 4922
- Dehnen W., Binney J.J., 1998, *MNRAS* 298, 387
- ESA, 1997, *The Hipparcos and Tycho Catalogues*, ESA SP-1200
- Edvardsson B., Andersen J., Gustafsson B., Lambert D.L., Nissen P.E., Tomkin J., 1993a, *A&A* 275, 101 (EAGLNT)
- Edvardsson B., Gustafsson B., Nissen P.E., Andersen J., Lambert D.L., Tomkin J., 1993b, in *Panchromatic View of Galaxies*, eds. Hensler, G., Theis, Ch. & Gallagher, J., p. 401
- Eggen O.J., Lynden-Bell D., Sandage A.R., 1962, *ApJ* 136, 748
- Feltzing S., Gustafsson B., 1999, *A&AS* 129, 237
- François P., 1996, *A&A* 313, 229
- Fuhrmann K., 1998, *A&A* 338, 161
- Fuhrmann K., Bernkopf J., 1999, *A&A* 347, 897
- Garz T., 1973, *A&A*, 26, 471
- Gratton R.G., Sneden C., 1987, *A&A* 178, 179
- Hannaford P., Lowe R.M., Grevesse N., Noels A., 1992, *A&A* 259, 301
- Holweger H., Heise C., Kock M., 1990, *A&A* 232, 510
- IAU 1999, in *Transactions of the IAU*, vol. XXIII B, ed. J.Andersen, p.141
- Johnson D.R.H., Soderblom D.R., 1987, *AJ* 93, 864
- Kostyk R.I., 1982, *Astrometriya Astrofiz.* 46, 58
- Lambert D.L., 1978, *MNRAS* 182, 249
- Lambert D.L., Warner B., 1968, *MNRAS* 138, 181
- Mäcke R., Holweger H., Griffin R., Griffin R., 1975, *A&A* 38, 239
- Magain P., 1987, *A&A* 181, 323
- Mashonkina L., Gehren T., Bikmaev I., 1999, *A&A* 344, 221
- Mihalas D., Routly P.M., 1968, *Galactic Astronomy*, (Freeman, San Francisco), p. 101
- Moore C.E., Minnaert M.G.J., Houtgast J., 1966, *The Solar Spectrum 2935 Å to 8770 Å*, National Bureau of Standards, Monograph 61, Washington
- Morris D.H., Mutel R.L., 1988, *AJ* 95, 204
- Nissen P.E., Edvardsson B., 1992, *A&A* 261, 255
- Nissen P.E., Schuster W.J., 1997, *A&A* 326, 751
- Nissen P.E., Chen Y.Q., Schuster W.J., Zhao G., 1999, *A&A* (in press)
- O'Brian T.R., Wickliffe M.E., Lawler J.E., Whaling W., Brault J.W. 1991, *J. Opt. Soc. Am. B* 8, 1185
- Olsen E.H., 1983, *A&AS* 54, 55
- Olsen E.H., 1988, *A&A* 189, 173
- Olsen E.H., 1993, *A&A* 102, 89
- Petit M., 1990, *A&AS* 85, 971
- Porte de Mello G.F., da Silva L., 1996, in: *Stellar Abundance*, eds. B. Barbuy, W.J. Maciel J.C. Gregórie-Hetem J.C. p. 59
- Rogers F.J., Iglesias C.A., 1992, *ApJS* 79, 507
- Reetz J., 1999, in: *Galaxy Evolution: Connecting the Distant Universe with the Local Fossil Record*, eds. M. Spite, F. Crifo, Kluwer (in press)
- Ryan S.G., 1998, *A&A* 331, 1051
- Samland M., 1998, *ApJ* 496, 155
- Schuster W.J., Nissen P.E., 1989, *A&A* 221, 65
- Simmons G.J., Blackwell D.E., 1982, *A&A* 112, 209
- Smith G., Raggett D.St.J., 1981, *J.Phys. B* 14, 4015
- Steffen M., 1985, *A&AS* 59, 403
- Takeda Y., Kato K.-I., Watanabe Y., Sadakane K., 1996, *PASJ* 48, 511
- Thévenin F., Idiart T.P., 1999, *ApJ* 521, 753
- Timmes F.X., Woosley S.E., Weaver T.A. 1995, *ApJS* 98, 617
- Tomkin J., Edvardsson B., Lambert D.L., Gustafsson B., 1997, *A&A* 327, 587
- Tomkin J., Lambert D.L., Balachandran S., 1985, *ApJ* 290, 289
- Tsujimoto T., Nomoto K., Yoshii Y., Hashimoto M., Yanagida S., Thielemann F.-K. 1995, *MNRAS* 277, 945
- Twarog B.A., 1980, *ApJ* 242, 242
- Unsöld A., 1955, *Physik der Sternatmosphären*, Springer-Verlag, Berlin
- VandenBerg D.A., Bell R.A. 1985, *ApJS* 58, 561
- VandenBerg D.A., Swenson F.J., Rogers F.J., Iglesias C.A., Alexander D.R., 1999 (in preparation)
- Wallerstein G., 1962, *ApJS* 6, 407
- Whaling W., Hannaford P., Lowe R.M., Biémont E., Grevesse N., 1985, *A&A* 153, 109
- Wickliffe M.E., Lawler J.E., 1997, *ApJS* 110, 163
- Wiese W.L., Martin G.A., 1980, in: *Wavelengths and Transition Probabilities for Atoms and Atomic Ions*, NSRDS-NBS 68, Washington, DC
- Zhao G., Butler K., Gehren T., 1998, *A&A* 333, 219
- Zhao G., Gehren T., 1999, in: *The Galactic Halo: from Globular Clusters to Field Stars*, the 35th Liège International Astrophysics Colloquium, eds. A. Noels, P. Magain (in press)